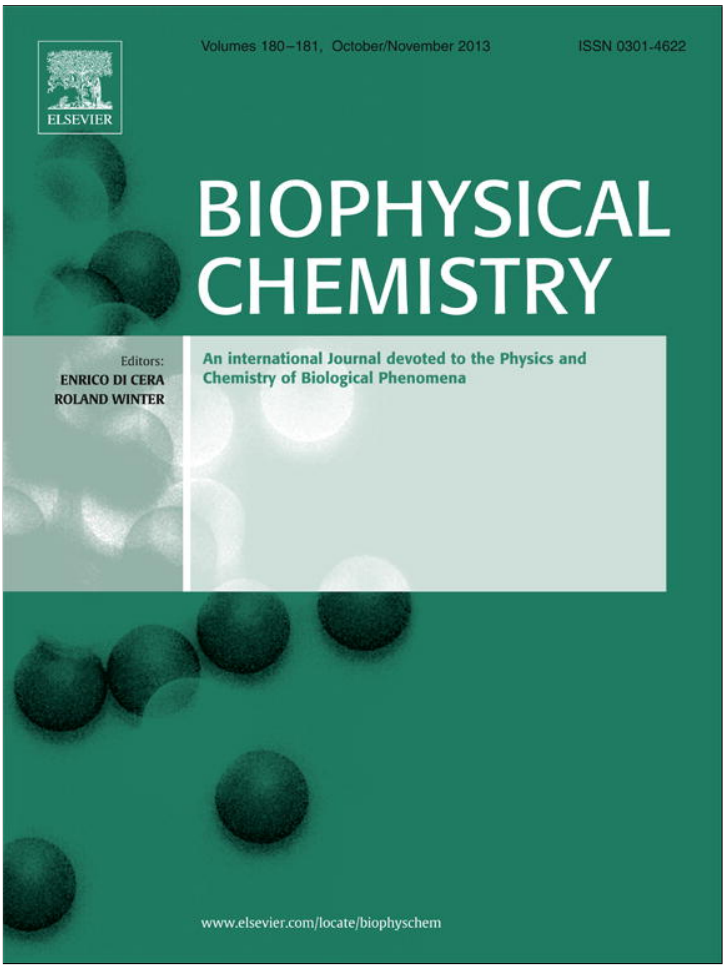

Biophysical Chemistry 180–181 (2013) 127–134

Contents lists available at ScienceDirect

Biophysical Chemistry

journal homepage: http://www.elsevier.com/locate/biophyschem

Charge transfer through DNA/DNA duplexes and DNA/RNA hybrids: Complex theoretical and experimental studies

Irena Kratochvílová [a,*], Martin Vala [b], Martin Weiter [b], Miroslava Špérová [b], Bohdan Schneider [c], Ondřej Páv [d,**], Jakub Šebera [a,d], Ivan Rosenberg [d], Vladimír Sychrovský [d]

[a] Institute of Physics, Academy of Sciences Czech Republic, v.v.i, Na Slovance 2, CZ-182 21, Prague 8, Czech Republic
[b] Materials Research Centre, Faculty of Chemistry, Brno University of Technology, Purkyňova 118, CZ-612 00 Brno, Czech Republic
[c] Institute of Biotechnology Academy of Sciences Czech Republic, v.v.i., Vídeňská 1083, CZ-142 20 Prague 4, Czech Republic
[d] Institute of Organic Chemistry and Biochemistry Academy of Sciences Czech Republic, v.v.i., Flemingovo náměstí 2, CZ-16610 Prague 6, Czech Republic

HIGHLIGHTS

- Study of charge transfer processes in short DNA/DNA and RNA/DNA duplexes with virtually equivalent sequences.
- Temperature dependent steady state and time-resolved fluorescence spectroscopy, Density Functional Theory.
- More effective charge transfer in RNA/DNA hybrids-delocalized HOMO and holes, specific base stacking and conformational flexibility.
- RNA/DNA and DNA/DNA charge transfer properties-connected with temperature affected structural changes.
- Charge transfer/fluorescence spectroscopy probe of even tiny changes of molecular structures and settings.

GRAPHICAL ABSTRACT

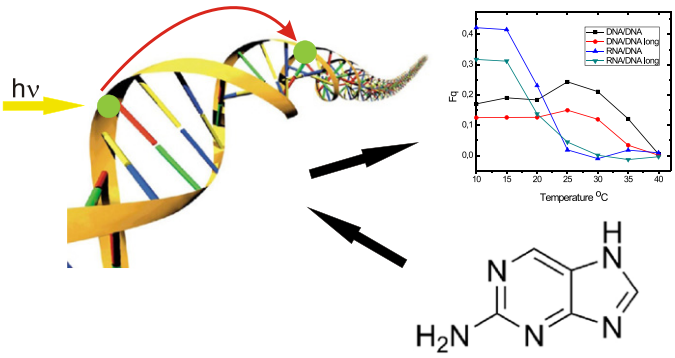

ARTICLE INFO

Article history:
Received 11 June 2013
Received in revised form 19 July 2013
Accepted 20 July 2013
Available online 31 July 2013

Keywords:
Charge transfer in oligonucleotides
Temperature dependent steady state fluorescence spectroscopy
Time-resolved fluorescence spectroscopy
Density Functional Theory
Electronic properties of biomolecules

ABSTRACT

Oligonucleotides conduct electric charge via various mechanisms and their characterization and understanding is a very important and complicated task. In this work, experimental (temperature dependent steady state fluorescence spectroscopy, time-resolved fluorescence spectroscopy) and theoretical (Density Functional Theory) approaches were combined to study charge transfer processes in short DNA/DNA and RNA/DNA duplexes with virtually equivalent sequences. The experimental results were consistent with the theoretical model — the delocalized nature of HOMO orbitals and holes, base stacking, electronic coupling and conformational flexibility formed the conditions for more effective short distance charge transfer processes in RNA/DNA hybrids. RNA/DNA and DNA/DNA charge transfer properties were strongly connected with temperature affected structural changes of molecular systems — charge transfer could be used as a probe of even tiny changes of molecular structures and settings.

* Corresponding author. Tel.: +420 266 052 524; fax: +420 286 890 527.
** Corresponding author. Tel.: +420 220 183 244; fax: +420 220 183 531.
E-mail addresses: krat@fzu.cz (I. Kratochvílová), pav@uochb.cas.cz (O. Páv).

0301-4622/$ – see front matter © 2013 Elsevier B.V. All rights reserved.
http://dx.doi.org/10.1016/j.bpc.2013.07.009

1. Introduction

The ability of oligonucleotides to mediate charge transfer is the basis of novel molecular devices and plays a role in the processes of sensing and/or repair of molecular damage. Charge transfer along or through these molecules has been investigated by various experimental techniques for over a decade, sometimes with contradictory results [1–15]. Oligonucleotides conduct electric charge via various mechanisms [6–9,16–28] (depending on many parameters) and their characterization and understanding is a very important and complicated task.

High charge transfer rate between elaborated donor–acceptor pairs in DNA [3,10,13] has triggered a series of direct electrical transfer measurements [1–5,15–31]. As far as the biological importance of oligonucleotide charge transfer is concerned Barton and co-workers found that the repair of a damaged base is controlled from a remote site via long-distance charge transfer [12,15] — DNA charge transfer can serve as an antenna for DNA damage, allowing proteins to monitor oxidation events that occur far away and respond to them quickly [32]. The extent of delocalization and the character of electronic states in DNA are believed to play an essential role in probing the electronic properties of a substrate during DNA repair; even its subtle deviations from normal DNA could probably be detected with different charge carrier mobility [1–5,10–16]. Specifically, the detection of oxidative damage in the regulation of tumor-suppressor genes such as p53 is believed to be controlled by charge transfer [10–16]. It has been also shown that the conductance of DNA is important for the functioning of enzymatic activity with possible biological consequences [13].

Here, we extended our previous studies [9,17] of charge transfer in DNA oligonucleotides with various base-pairing patterns. The main goal of this contribution was to compare the charge transfer mechanism of the standard DNA/DNA and hybrid DNA/RNA duplexes. We wanted to show how the states and conformations of oligonucleotide chains might affect charge transfer. For this purpose we employed temperature dependence of steady state fluorescence spectroscopy, time-resolved fluorescence spectroscopy [33], melting temperature measurements, as well as theoretical approaches within Density Functional Theory (DFT) and proposed how short distance charge transfer efficiency in oligonucleotides is affected by molecular structure, temperature stability of the systems, chain flexibility, holes, base interactions, and charge distributions [28–56]. Our results highlighted in detail the interplay between the efficiency of charge transfer and basic physico-chemical properties of natural oligonucleotides, which has a significance not only for biochemistry and biology but also for the future utilization of these materials in nanotechnology [48–62].

2. Materials and methods

2.1. Sample preparation

Four general types of duplexes were prepared: DNA/DNA composed of two DNA strands, and RNA/DNA composed of complementary RNA and DNA strands, where the donor–acceptor pairs: 2-aminopurine (Ap)–guanine (G), were separated by two or three bases (long oligonucleotides in our nomenclature) – Table 1, chemical structure – Fig. S1 in Supporting materials. The duplexes containing the Ap–G pair are called redox active. In all measurements, Ap represented an optically excited fluorescent redox probe introduced into the DNA chain as a hole donor [20,21]. The charge developed upon excitation transferred from Ap to the redox counterpart was trapped by hole acceptor G. The DNA/DNA and RNA/DNA duplex contained one Ap paired with thymine (T) and uracil (U), respectively [20,22]. The fluorescence spectroscopy measurements performed for the redox active duplexes were compared with measurements of redox inactive duplexes in which the hole acceptor G was replaced by redox-inactive inosine (I).

The oligonucleotides listed in Table 1, Fig. S1 Supplementary material were synthesized using the standard phosphoramidite protocol. The synthesis was performed on a 1 μmol scale on a 5-*O*-dimethoxytrityl-1-(6-*N*-benzoyladenin-9-yl)-β-*D*-ribofuranos-3-*O*-succinyl LCAA-CPG using a GenSyn V02 RNA/DNA synthesizer. 2-aminopurine and inosine units were incorporated using commercial phosphoramidites purchased from Glen Research.

Table 1
The DNA/DNA and RNA/DNA duplexes for optical spectroscopy measurements. In the redox active duplexes, the hole acceptor was guanine (G) and the hole donor was 2-aminopurine (Ap). In the redox inactive duplexes, G was replaced by redox-inactive inosine (I). Other symbols indicate normal nucleic acid bases in the oligonucleotide sequences.

Sample description	Sequence
DNA/DNA redox active	**5′-d(TIA ITAp AAG TTA IA)-3′**
DNA/DNA redox inactive	**3′-d(ACT CAT TTC AAT CT)-5′**
	5′-d(TIA ITAp AAI TTA IA)-3′
	3′-d(ACT CAT TTC AAT CT)-5′
RNA/DNA redox active	**5′-d(TIA ITAp AAG TTA IA)-3′**
RNA/DNA redox inactive	**3′-r(ACU CAU UUC AAU CU)-5′**
	5′-d(TIA ITAp AAI TTA IA)-3′
	3′-r(ACU CAU UUC AAU CU)-5′
DNA/DNA long redox active	**5′-d(TIA ITAp AAAG TTA IA)-3′**
DNA/DNA long redox inactive	**3′-d(ACT CAT TTTC AAT CT)-5′**
	5′-d(TIA ITAp AAAI TTA IA)-3′
	3′-d(ACT CAT TTTC AAT CT)-5′
RNA/DNA long redox active	**5′-d(TIA ITAp AAAG TTA IA)-3′**
RNA/DNA long redox inactive	**3′-r(ACU CAU UUUC AAU CU)-5′**
	5′-d(TIA ITAp AAAI TTA IA)-3′
	3′-r(ACU CAU UUUC AAU CU)-5′

After the solid-phase synthesis, a column was inserted into the pressure vessel and treated with gaseous ammonia (0.7 MPa) for 16 h to remove the acyl protecting groups and to release the product from solid support. Finally, unprotected molecules were washed out from the column by 0.1 M TEAA buffer, purified, and characterized by preparative ionic exchange chromatography (DNAPac, Dionex). For details, see Supporting material S4 and Fig. S2.

The melting temperature measurements were performed on a CARY 100 Bio UV Spectrophotometer (Varian Inc.) equipped with a Peltier temperature controller and thermal analysis software (Fig. S2, in Supporting material). The samples were prepared by mixing the complementary strands together in 100 mM NaCl, 50 mM NaH_2PO_4, and 1 mM EDTA (pH 7.2) to afford a final concentration of 4 μM. A temperature gradient of 1 °C/min was applied. Tm values were determined from the maximum of the first derivative of the absorbance/temperature plots (Tm ± 0.5 °C).

For optical measurements the synthesized oligomers were dissolved in 50 mM sodium phosphate buffer (pH = 7); the final duplex concentration was 5 μM. UV–vis spectroscopy was performed with a Varian Carry 50. As Ap made a band in the 300–340 nm range in absorption spectra it was possible to selectively excite the Ap. On the basis of the comparable Ap absorbance for all measured samples (0.023 ± 0.001) at 320 nm, the same oligonucleotide concentration was confirmed.

2.2. Fluorescence spectroscopy

Spectroscopic techniques were used to probe charge transfer efficiency in DNA/DNA duplexes and RNA/DNA hybrids containing photoexcited 2-aminopurine. DNA/DNA duplexes and RNA/DNA hybrid fluorescence were measured at temperature scale from 10 to 40 °C in a series of samples containing redox-inactive and redox-active duplexes. Specially, to distinguish the fluorescence quenching originating from charge transfer and the fluorescence quenching arising from different processes, the spectroscopic measurements were calibrated against redox-inactive duplexes, where G was replaced by inosine. The fluorescence spectroscopy was performed with Fluorolog Horiba JY with double monochromators for excitation and emission. The steady state emission spectra were obtained by exciting at 320 nm, the excitation spectra were measured at 365 nm. The excitation in time-resolved

fluorescence spectroscopy was performed at 329 nm with a laser diode and a pulse duration <1 ns, and the fluorescence was recorded at the Ap maximum, 365 nm.

The emission of photoexcited Ap was monitored over a 120-ns time regime using the single photon counting method (TCSPC, Fluorocube Horiba JY) for redox inactive and redox active oligonucleotides. The decay of the time-resolved fluorescence of photoexcited Ap was fitted in a three-exponential fashion in accordance with methodology published in [20,21], yielding three lifetimes and three amplitudes. The different lifetimes corresponded to different modes and/or efficiencies of fluorescence quenching, which can, according to the literature [18,19,63–66], be related to different conformers.

2.3. Computational details

The structural models in the theoretical calculations consisted of four oligonucleotide base pairs: the base pair containing the G acceptor, the pair containing the Ap donor, and the two base pairs between them as they appeared in the redox active duplexes (Table 1).

The DNA/DNA and DNA/RNA duplexes were represented by structural models found in structural databases. The two structural models for the DNA/DNA and RNA/DNA duplexes reflected the actual geometry of oligonucleotides found in structural databases [30]. The DNA/DNA model was derived from the structure of the DNA duplex with PDB ID 2G1Z the RNA/DNA one from the structure of a PDB ID 219D [31]. In fact, only the backbone parts of selected molecules were adopted for structural models while nucleobases were modified according to the duplexes in Table 1. The structural fragment of the DNA/DNA backbone of 2G1Z can be characterized as a B-form while the RNA/DNA backbone fragment from 219D was characterized as conformational mixture of A-forms.

The geometry of models was gradient optimized keeping the initial backbone geometry fixed to preserve the B- and A-form of the DNA/DNA and RNA/DNA models, respectively. The Density Functional Method (DFT) employing the DFT-B97D [34] functional with the D3 Grimme's dispersion correction [35] and atomic basis set def2-SVP [36,37] were used in the geometry optimizations. The RI approximation [38] (the resolution of identity) employing the auxiliary basis sets [39] was imposed in all B-97D calculations. Hydration effects were calculated by using the implicit water solvent model COSMO [40] (the Conductor-like Screening Model) or PCM [41] (Polarizable Continuum Model). The geometry optimizations were performed using the Turbomole-6.3 quantum chemistry program package [42]. The oligonucleotide sequences were set according to Table 1. The hydrogen atoms were added and each model was augmented with six Na^+ ions coordinated to the backbone phosphates (Fig. 1).

Electric dipole moment and electronic coupling were calculated using the DFT functional M05-2X [43,44] and 6-31G(d) [45] basis set (the Gaussian 09 program package [46]). The excited states, transition moments, and molecular orbitals were calculated using the time dependent DFT method (TD-DFT) [38] in the scope of the DFT B3LYP functional [47,48]. Hole delocalization was calculated as the distribution of charge and electron spin density. The optimized geometries of neutral oligonucleotides (see Fig. 1) were used for the investigation of charge and spin density distribution. For the Mulliken charge modeling the TD-DFT/B3LYP/6-31G(d)/PCM calculation of excited states was used. From the analysis of Mulliken charges for bases, the difference between the charges for the ground and excited states was obtained. We supposed that the differences in the Mulliken charge were indicative of the formation of a hole immediately after excitation. For spin density analysis we used DFT/B3LYP/6-31G(d)/PCM single point calculations of the cation radical state computed for the optimal geometry of the neutral duplex. The spin density distribution in percents showed the delocalization of holes at bases (specifically the G base/hole acceptor) — for details see [49]. Our models of charge distribution show delocalization of charges (holes) in DNA/DNA duplexes and RNA/DNA hybrids. Based on the works of Conwell et al. [50–53] we can suppose that the delocalization of hole and polaron (important phenomenon for charge transport in organic materials) is closely related to each other.

The electronic coupling between two neighboring DNA bases was calculated using the two-state Generalized Mulliken–Hush (GMH) method [54–57]. For recent applications of the GMH method see studies on photoinduced charge transfer in DNA hairpins [58] and π-stacked porphyrin-bridge-quinone systems [59]. The electronic coupling was calculated for the purine bases of the ApAAG DNA strand (actually appeared in both models). Two tetramers and all dimers consisting of adjacent consecutive pairs of bases were extracted from the optimized geometries of the DNA/DNA and RNA/DNA duplexes. Only the local

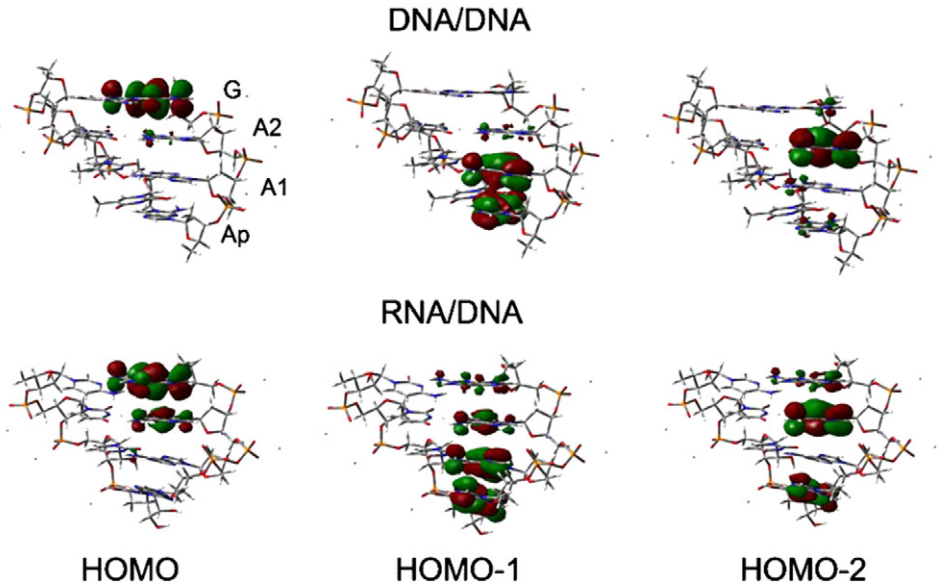

Fig. 1. Spatial distribution of the highest occupied molecular orbitals (HOMO) calculated in DNA/DNA and RNA/DNA model duplexes ordered according to their energies. The orbitals were localized at the purine-rich ApAAG strand. The HOMO orbital was dominantly localized at G, HOMO-1 at Ap and neighboring A, and HOMO-2 at A next to the G base. The oligonucleotide sequences were set according to Table 1. The hydrogen atoms were added and each model was augmented with six Na^+ ions coordinated to the backbone phosphates.

geometry of bases obtained in the geometry optimization of the whole duplex was preserved in the GMH calculations. Within the two-state GMH method, the electronic coupling for two adjacent bases B1 and B2 is expressed as

$$V_{B1B2} = (E_2 - E_1)\frac{|\mu_{12}|}{\sqrt{(\mu_1 - \mu_2)^2 + 4\mu_{12}^2}} \quad (1)$$

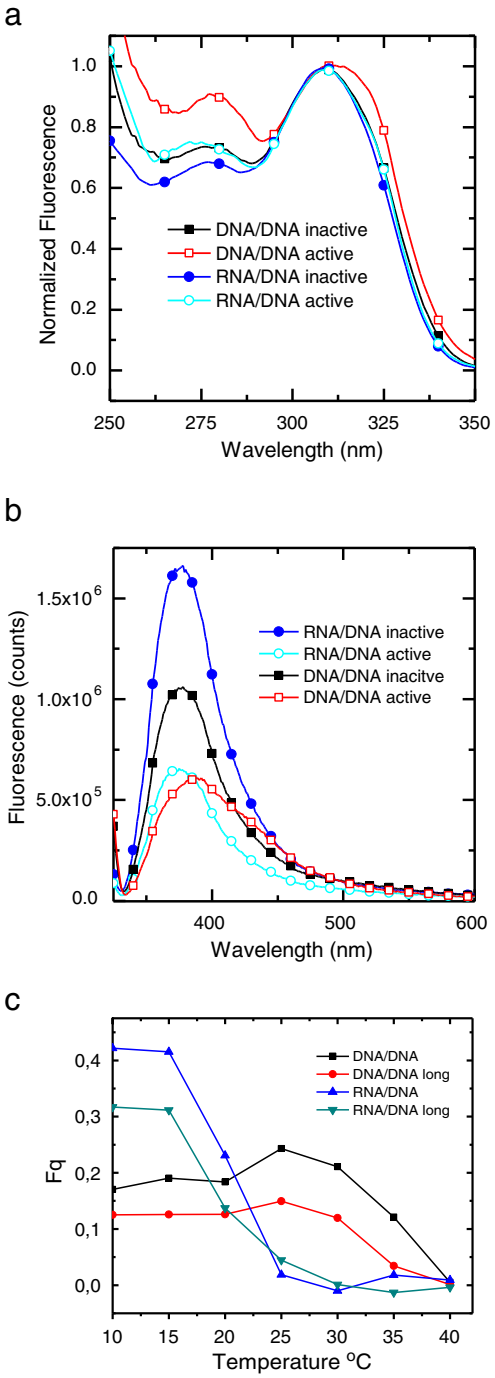

Fig. 2. a). The excitation spectra of DNA/DNA and RNA/DNA duplexes measured for both redox active and inactive forms at 10 °C, normalized to curves maximum values. b). The fluorescence emission spectra of DNA/DNA and RNA/DNA duplexes measured for both redox active and inactive forms at 10 °C. c). Temperature dependent yield of charge transfer for DNA/DNA and RNA/DNA duplexes with various separation of Ap (donor) and G (acceptor) by adenosine units. 3 adenosine units: RNA/DNA long, DNA/DNA long, 2 adenosine units: RNA/DNA, DNA/DNA.

where $(E_2 - E_1)$ is the vertical excitation energy, μ_1 and μ_2 are the dipole moments for the ground and electronic excited state calculated for the dimer cation. μ_{12} is the transition dipole moment calculated for transition between two electronic states (ground and first excited state) of dimer cation. In this approach, HOMO and HOMO-1 (for neutral dimer system) were transformed to HOMO(β) and LUMO(β) and HOMO(α) and HOMO-1(α) (for cation dimer system). The electron was transferred (excited) from HOMO(β) to LUMO(β) orbital. In a system where charge transfer between donor and acceptor was mediated by a bridge, such as by the middle AA segment in our case, the electronic coupling V_{DA} between donor base D and acceptor base A was calculated by using the superexchange approach [56,60,61],

$$V_{DA}(SE) = \frac{V_{D1}V_{12}V_{2A}}{(E_t - E_1)(E_t - E_2)} \quad (2)$$

where the energy E_t is average of HOMO and HOMO-1 energies (donor and acceptor levels of neutral tetramer system), E_1 and E_2 are the HOMO-2 and HOMO-3 (bridge states for neutral tetramer system) and V_{D1}, V_{12}, and V_{2A} are electronic couplings for adjacent D (donor), 1 and 2 (bridge), and A (acceptor) bases.

3. Results

3.1. Fluorescence spectroscopy

The excitation spectra of both active and inactive duplexes were composed of two main bands. The longer wavelength band (maximum at 309 nm) represents the main excitation pathway and overlaps the absorption of Ap (Fig. 2). The shorter wavelength excitation band with a maximum around 275 nm arose from singlet–singlet energy transfer from bases adjacent to Ap [23–25]. The stronger the relative intensity of this band was, the better the base stacking interaction of Ap within the DNA strand could be anticipated, which means that Ap was better incorporated in the double helix [18,19]. The intensity measured for the RNA/DNA hybrid was slightly smaller than that for the DNA/DNA. From measured fluorescence emission spectra (Fig. 2b) the relative fluorescence intensities (with respect to the intensity obtained for free Ap) were expressed for redox active (Φ_G) and inactive molecules (Φ_I). The redox inactive duplex contained just the hole donor Ap while the redox active one contained the donor–acceptor pair Ap–G. The fluorescence quenching efficiencies (Table 2) were calculated as $F_q = 1 - \Phi_G / \Phi_I$. Fluorescence emission intensities were measured at temperatures from 10 to 40 °C for DNA/DNA and RNA/DNA duplexes with various distance (2–3 adenosine units) between the donor and acceptor (Fig. 2c, Table 2). All studied duplexes had a higher overall quenching of fluorescence (indicating better charge transfer properties) for the hybrid RNA/DNA rather than the DNA/DNA sequences of corresponding lengths. Importantly, the lowering of redox active fluorescence as compared to redox inactive fluorescence confirmed donor–acceptor charge transfer for DNA/DNA and RNA/DNA. At the same time, longer distance between the Ap and G leads in all cases to smaller charge transfer yield — this effect also confirmed donor–acceptor charge transfer [29].

Table 2
The temperature dependence of quenching efficiencies (F_q) for DNA/DNA and RNA/DNA duplexes with two or three (long) adenosine units between the donor and acceptor.

Temp	DNA/DNA	DNA/DNA long	RNA/DNA	RNA/DNA long
°C	F_q	F_q	F_q	F_q
10	0.2006	0.1271	0.4218	0.3171
15	0.1906	0.1258	0.4154	0.3114
20	0.1838	0.1321	0.2307	0.1372
25	0.2431	0.1565	0.0186	0.0444
30	0.2108	0.1197	−0.0099	0.0010
35	0.1212	0.0345	0.0181	−0.0132
40	0.005	0.0012	0.0091	−0.0038

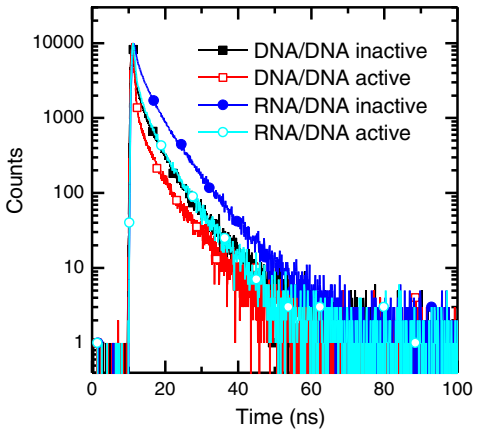

Fig. 3. The time resolved luminescence of DNA/DNA and RNA/DNA duplexes measured for redox inactive and redox active forms at 10 °C. The luminescence measured with the Time Correlated Single Photon Counting method is depicted on a semi-logarithmic scale.

Significant dependence of charge transfer yield on temperature was also observed. As the temperature increased, the enhanced dynamics affected/improved the DNA/DNA mediated charge transfer — the DNA/DNA charge transfer efficiency increased continually. At the temperature near the melting point (30.5–32 °C, see Fig. S2) charge transfer dropped down — this could be attributed to conformation changes during melting of the duplex. For the DNA/RNA hybrids, charge transfer yield began to decrease at lower temperatures, near 20 °C, in good correlation with lower melting temperatures (24–25 °C, see Fig. S2) of these duplexes.

Our interpretation of fluorescence decay data (Fig. 3) was based on multiexponential fit. Recently, the multiexponential analysis of fluorescence decays has been preferred (in similar cases) [26,27]. For our data which were obtained with resolution of TCSPC apparatus (Fluorocube Horiba JY) the three-exponential fit gave best results: satisfactory reduced chi-square and weighted residuals uniformly distributed about zero. Either four/two exponential fit or continuous distribution of decay times led to unsatisfactory precision.

Based on previous works [2,26,27] we could suppose that for parameters obtained from multiexponential fit of fluorescence decays the shortest fluorescence lifetime (τ_1 in Table 3) should reflect the hole donor/Ap fraction that is best incorporated into the duplex [2,26,27] and non-radiative recombination could play a dominant role due to Ap being well incorporated into the double helix. The second lifetime (τ_2 in Table 3) is assumed to capture the fraction of partially stacked Ap, and the longest one, the fraction of Ap incorporated less well into the helix [2,26,27]. According to this hypothesis, the difference between redox free and redox active RNA/DNA relative fractions A_1–A_3 can be associated with duplex conformational flexibility: the relative amount of worse stacked Ap, A_3, was lower for RNA/DNA active duplexes, which indicates the higher conformational flexibility of RNA/DNA duplexes compared to DNA/DNA ones. Smaller differences between redox inactive and redox active relative fractions for the DNA/DNA duplexes are coherent with their more compact structures and less conformational flexibility. This is in accord with the previous studies [18,19,28,29]. It should be noted that the best Ap stacking in active DNA/DNA duplexes (the mostly pronounced shorter excitation wavelength band, see Fig. 2a, the fastest fluorescence decay, see Fig. 3) could influence/cause the specific active DNA/DNA emission spectrum (Fig. 2b).

Table 3
The fluorescence lifetimes (τ_1 τ_2, τ_3) and relative amplitudes (A_1, A_2, A_3) fitted as a three-exponential function of the measured overall decays in Fig. 3, measured at 10 °C.

Duplex	τ_1 (ns)	A_1 (%)	τ_2 (ns)	A_2 (%)	τ_3 (ns)	A_3 (%)
DNA/DNA redox inactive	0.11	44.70	2.18	26.17	6.60	29.14
DNA/DNA	0.09	67.62	1.91	13.74	6.48	18.65
RNA/DNA redox inactive	0.23	19.69	2.68	36.61	7.13	43.70
RNA/DNA	0.06	64.65	2.40	17.86	6.54	17.49

The introduction of redox active G into sequences resulted in a change of the lifetimes and relative amplitudes of fluorescence (Table 3). The most pronounced effect was fitted for the shortest lifetime that decreased (and the relative amplitude increased) in both redox active duplexes. The effect is more pronounced for the RNA/DNA hybrid showing that the charge transfer was more effective through the hybrid than DNA/DNA duplexes. All fits of these measurements indicated an enhancement of the Ap quenching connected with charge transfer.

3.2. Melting temperature measurements

Typically, the DNA/DNA duplex is a B-type duplex and the RNA/DNA duplex is an A-type duplex. In RNA/DNA hybrids the RNA strand induces the duplex conformation into the A-form [47–49, 67]. Our melting temperature measurements showed that in both cases the RNA/DNA hybrid (active) melted at lower temperatures than the DNA/DNA (active) duplexes (Supporting material, Fig. S2). The higher melting temperatures of the DNA/DNA duplexes correspond to their higher stability and more effective stacking in the B-form [18,19].

3.3. Computer modeling

The calculated energies of HOMO orbitals and their appearance and localization in the model structures were indicative of the charge transfer efficiency between the donor Ap and the acceptor G. The HOMO, HOMO-1, and HOMO-2 orbitals were localized exclusively at the purine-rich ApAAG DNA strand (Fig. 1). The AA segment was specially designed in this study to bridge the donor with the acceptor, as purine bases form a better electronic bridge in comparison with pyrimidines. Because the sequences of DNA strands appearing in both DNA/DNA and RNA/DNA molecules were the same, the calculated differences in HOMO orbitals had to be induced by the complementary CTTT DNA and CUUU RNA strands.

The HOMO orbital was dominantly localized at acceptor G in both duplexes, but its partial localization at the adjacent A base was also calculated especially for the RNA/DNA molecule. The HOMO-1 was mainly localized at donor Ap and partially also at the AA bridge. The partial delocalization was again more pronounced for the RNA/DNA duplex. The HOMO-2 was dominantly localized at the bridging A base next to G, and in the RNA/DNA molecule it was also localized on acceptor Ap. The ordering of HOMO orbitals in both molecules was the same as regards their orbital energies and also their localizations at individual bases were similar (Table 4, Fig. 1). However, the HOMO orbitals in RNA/DNA were all more delocalized along the strand as compared with those in normal DNA/DNA. We can therefore assume that the electronic perturbation induced by the complementary DNA or RNA strand in the ApAAG DNA strand was relatively modest.

The electronic couplings for the pairs of adjacent bases and also those for the donor–acceptor pair in the ApAAG strand of DNA/DNA and RNA/DNA molecules differed (Table 5). The electronic coupling between Ap and the adjacent A base V_{AAp} in RNA/DNA was smaller by 0.045 eV than that in DNA/DNA. The rest of the electronic couplings in RNA/DNA were larger, V_{AA} by 0.082 eV and V_{GA} by 0.079 eV. Also, the donor–acceptor coupling $V_{GAp}(SE)$ in the RNA/DNA molecule was larger by 0.038 eV. The $V_{GAp}(SE)$ coupling depended on all couplings for adjacent pairs (Eq. (2)) and its larger value in the RNA/DNA molecule can be thus explained with larger values of V_{AA} and V_{AAp} couplings. Similar values of V_{AA} couplings were calculated previously by Reha et al. [62]: 0.11 eV in the A-DNA duplex, while in B-DNA, where bases overlapped less, it was only 0.09 eV. Bases in the A-form have a larger overlap than bases in the B-DNA, which may explain the calculated trends in electronic couplings.

Table 4
The orbital energies of HOMO and LUMO orbitals in eV calculated using the B3LYP/6-31G(d) method in model duplexes. The dominant orbital localization is shown in parenthesis (and depicted Fig. 1) for the individual bases of the Ap–A1–A2–G DNA or the complementary strand.

Duplex	LUMO+1	LUMO	HOMO	HOMO-1	HOMO-2	HOMO-3	HOMO-4
DNA/DNA	−1.12 (Ap)	−1.15 (C + T)	−5.48 (G)	−5.64 (Ap + A1)	−5.75 (A2)	−6.02 (T + T + T)	−6.05 (Ap + A1)
RNA/DNA	−1.14 (Ap)	−1.16 (U + U)	−5.51 (G)	−5.68 (Ap + A1 + A2)	−5.81 (Ap + A2)	−6.01 (Ap + A1)	−6.32 (C)

To describe the local geometry and arrangement of bases in DNA/DNA and RNA/DNA molecules, we measured the distances of a few selected atoms in one base from the idealized plane defined by inner-ring atoms of an adjacent base. The distances for C8, N9, N7, N1, O6 and N3 inner-ring atoms measured in adjacent pairs of the ApAAG strand roughly revealed their mutual orientation (Fig. S3 in Supporting materials). The standard IUPAC numbering of atoms for purine bases was used. Two geometrical characteristics can be estimated from the measured distances: the overall distance and the mutual inclination of the bases. In addition, the mutual spatial overlap of the bases can be seen roughly in Fig. S3, when considering the projections of selected atoms into an idealized plane.

The distances between the inner-ring atoms of the G and neighboring A bases in two duplexes were similar and ranged from 3.0 Å to 3.3 Å. The distance between the bases in DNA/DNA was somewhat larger, which may explain the larger V_{GA} coupling, the distance between the bases of the AA pair was much larger with distances ranging from 4.2 Å to 3.0 Å in RNA/DNA and from 3.3 Å to 2.9 Å in DNA/DNA. The mutual overlap of the AA bases was larger in RNA/DNA, which explained the larger V_{AA} coupling. The mutual orientation of the AAp bases was nearly parallel, their distances ranged from 3.2 Å to 3.4 Å in RNA/DNA and from 3.1 Å to 3.2 Å in the DNA/DNA molecules. However, the spatial overlap was greater in DNA/DNA. The slightly closer proximity of bases in the AAp pair and their better overlap in DNA/DNA explained the larger V_{AAp} coupling.

The larger $V_{GAp}(SE)$ coupling in the RNA/DNA molecule was obtained due to the V_{AA} coupling for the AA bridge, which was explained by the better overlap of AA bases. The calculated electronic couplings depended on the overlap of bases and their mutual declination and distance. Because all these geometrical parameters were on average more favorable in RNA/DNA, the respective donor–acceptor electronic coupling $V_{GAp}(SE)$ was larger than that for DNA/DNA. The trend calculated for $V_{GAp}(SE)$ couplings in the two duplexes was consistent with the measurements of charge transfer.

The HOMO orbitals and the electronic couplings are both indicative of charge transfer efficiency in molecules. The HOMO orbitals calculated in DNA/DNA and RNA/DNA molecules were exclusively grouped along the purine-rich ApAAG DNA strand. In the RNA/DNA molecule, the HOMO orbitals were more delocalized as compared to those in the DNA/DNA molecule. The local geometries of the ApAAG strand in DNA/DNA and RNA/DNA were different. The spatial overlap of adjacent bases and their mutual declination and distances in the RNA/DNA molecule were overall more favorable with respect to the calculated electronic coupling. The V_{GA} and V_{AA} electronic couplings were larger in the RNA/DNA molecule, while the V_{AAp} was larger in the DNA/DNA molecule. The donor–acceptor $V_{GAp}(SE)$ electronic coupling was larger in the RNA/DNA molecule. The measured trends in charge transfer for normal DNA/DNA and hybrid RNA/DNA molecules were in agreement with the values of the calculated electronic coupling $V_{GAp}(SE)$. The calculations suggested more efficient hole transfer in the RNA/DNA hybrid molecule owing to the more delocalized nature of HOMO orbitals along the purine-rich ApAAG DNA strand and the better electronic coupling between donor and acceptor.

Low-lying excited states involved electronic transitions mainly between the HOMO-1 and LUMO+1 molecular orbitals (Table S1). The calculated electronic transitions for DNA/DNA (320 nm) and RNA/DNA (315 nm) corresponded to the experimental value ~ 320 nm. Electron excitation occurred essentially at the Ap and A1 bases; however, in the case of RNA/DNA, it even occurred at the A2 base. The excited state was preferably localized at the Ap base (Table 4).

The spin density distribution for the cation radical state showed a hole dominantly localized at G, but its delocalization was quite large, involving also the Ap, A1, and A2 bases (Table S2). Both charge and spin density calculations showed a slightly more delocalized hole in the case of the RNA/DNA hybrid. The more delocalized hole increases the hole transfer rate due to a smaller reorganization energy [52]. According to these results, hole transfer through the RNA/DNA hybrid should be more efficient than that through the DNA/DNA duplex.

Table 5
The electronic couplings in eV calculated for the adjacent pairs of bases in the ApAAG strand in DNA/DNA and RNA/DNA duplexes.

Duplexes	V_{GA}[a]	V_{AA}[a]	V_{AAp}[a]	$V_{GAp}(SE)$[b]
DNA/DNA	0.031	0.080	0.287	0.010
RNA/DNA	0.110	0.162	0.242	0.048

[a] Eq. (1) in Computational details.
[b] Eq. (2) in Computational details.

4. Discussion

Our experimental and theoretical data highlighted details between charge transfer efficiency, local geometry, conformational flexibility, and the electronic structure of the duplexes. The fluorescence spectroscopy detected higher fluorescence quenching of the RNA/DNA hybrid duplex indicating its better charge transfer compared to DNA/DNA (of corresponding lengths). The longer distance (3 adenosine units) between the Ap and G leads in all cases to smaller charge transfer yield — this effect confirmed charge transfer between donor and acceptor and support the superexchange charge transfer model [29]. With increasing temperature (below melting point) the temperature enhanced base dynamics affected (improved) the DNA/DNA mediated charge transfer [29]. The charge transfer efficiency dropped down to negligible values near and above the melting temperature, apparently because of the disruption of the regular double helical structure.

For RNA/DNA hybrids charge transfer yield decreased from 20 °C to melting point — RNA/DNA hybrids have at low temperatures best setting for charge transfer (confirmed by DFT modeling — interstrand stacking, more delocalized HOMO orbitals, more delocalized charge and holes, and better electronic coupling) which is at relatively low temperatures destroyed by changes connected with specific melting procedure. It was shown that RNA/DNA and DNA/DNA charge transfer temperature sensitivities are connected with temperature enhanced system dynamics, different temperature stabilities and different melting procedures of both systems. Charge transfer in this situation works as probe of even tiny changes in original system setting.

Conformationally more flexible RNA/DNA hybrids have larger interstrand stacking, more delocalized HOMO orbitals, more delocalized charge and holes, and better electronic coupling which all mean better conditions for charge transfer [17,68]. Enhanced mobility of the bases within the RNA/DNA hybrids gives the bases greater access to conformations and thus increases the probability of achieving conditions for charge transfer [2,64]. The larger conformational flexibility of the hybrid duplexes also causes larger delocalization of the holes that have a strong impact on the charge transfer process. The electronic overlap between bases within the hole is even larger, because the hole is formed in

response to a need for electron donation. As a consequence of all these effects, the charge in RNA/DNA hybrids becomes more delocalized. In this case, charge is more effectively transferred coherently from "donor" to "acceptor" through the intervening "bridging" nucleobases. But for temperatures above 20 °C due to RNA/DNA hybrids very specific properties (interstrand stacking, more delocalized HOMO orbitals, more delocalized charge and holes, better electronic coupling, conformational flexibility) the system setting is destroyed (related to melting procedure) and the charge transfer ability of the hybrids is falling down.

In contrast, DNA/DNA duplexes have not so conformationally flexible chain as RNA/DNA hybrids, more localized nature of HOMO orbitals, localized charge and hole plus worse electronic coupling. Under these conditions the DNA/DNA charge transfer could be with high probability more incoherent then charge transfer through RNA/DNA. The DNA/DNA charge transfer efficiency change with temperature in different way: charge transfer is rising up with temperature up to the melting point where the chain charge transfer efficiency of destroyed duplex falls down.

As possible applications of this work is concerned, strong relationship between fine deviations of base settings, phonons (temperature dependent dynamics) and oligonucleotide charge transfer conditions should be taken into consideration. Charge transfer measurements/fluorescence spectroscopy can be used as a probe of even tiny and quick changes of oligonucleotide structure, setting and interactions coming from various (biological/biochemical) origins.

5. Conclusions

In this work, experimental and theoretical approaches (temperature dependent time-resolved and steady state fluorescence spectroscopy, melting point measurements, and Density Functional Theory) were combined to gain insight into the process of charge transfer in DNA/DNA and RNA/DNA duplexes with various separation of Ap (donor) and G (acceptor) by adenosine units. The fluorescence spectroscopy measurements detected higher fluorescence quenching, indicating better charge transfer for the RNA/DNA hybrid duplex. The longer distance between the donor and acceptor caused lower charge transfer yield — this effect also confirmed charge transfer between donor and acceptor and support possible superexchange charge transfer model [24]. For DNA/DNA samples the charge transfer efficiency increased (due to temperature enhanced dynamics) up to temperatures close to the melting point where the charge transfer efficiency dropped as the duplex conformations change. RNA/DNA hybrids have different temperature stabilities — we observed charge transfer yield temperature dependence without significant increase but with charge transfer yield decrease practically from 20 °C to melting points. RNA/DNA and DNA/DNA charge transfer temperature sensitivities are connected with temperature enhanced dynamics, different temperature stabilities and different melting procedures of both systems. Charge transfer in this situation works as probe of even tiny changes in original system setting.

DFT modeling showed that in the case of hybrid duplex HOMO orbitals were more delocalized along the strand and that spatial overlap between adjacent bases was better, which all resulted in large values of electronic coupling. Also, charge and spin density analysis suggested a more delocalized hole in the RNA/DNA hybrid duplex. All the theoretical data obtained consistently indicated better charge transfer properties for the RNA/DNA hybrids. Based on our results, we suggested that charge could be transferred from donor to acceptor according to these mechanisms: in DNA/DNA duplexes, less effective incoherent charge transfer plays more important role; in RNA/DNA hybrids more effective coherent charge transfer should predominate.

Our results highlighted in detail the interplay between the efficiency of charge transfer and basic physico-chemical properties of natural oligonucleotides, which has a significance not only for biochemistry and biology but also for the future utilization of these materials in nanotechnology [69]. Charge transfer measurements can be used as very sensitive probe of oligonucleotide states and their changes coming from a wide range of (biological/biochemical) origins.

Acknowledgments

We gratefully acknowledge the support by grants No. 13-27676S, 205/10/2280, P304/10/1951, TA01011165, CZ.1.07/2.3.00/20.0306. The support by grant No. 202/09/0193 (Czech Science Foundation) under the IOCB's research project RVO: 61388963 is also gratefully acknowledged. Computer time at the MetaCentrum Brno is also gratefully acknowledged.

Appendix A. Supplementary data

Supplementary data to this article can be found online at http://dx.doi.org/10.1016/j.bpc.2013.07.009.

References

[1] R.E. Holmlin, P.J. Dandliker, J.K. Barton, Charge transfer through the DNA base stack, Angewandte Chemie International Edition 36 (1997) 2714–2730.
[2] M.E. Nunez, D.B. Hall, J.K. Barton, Long-range oxidative damage to DNA: effects of distance and sequence, Chemistry & Biology 6 (1999) 85–97.
[3] M.R. Arkin, E.D.A. Stemp, R.E. Holmlin, J.K. Barton, A. Hormann, E.J.C. Olson, P.F. Barbara, Rates of DNA-mediated electron transfer between metallointercalators, Science 273 (1996) 475–480.
[4] G.B. Schuster, Long-range charge transfer in DNA: transient structural distortions control the distance dependence, Accounts of Chemical Research 33 (2000) 253–260.
[5] D. Porath, A. Bezryadin, S. de Vries, C. Dekker, Direct measurement of electrical transport through DNA molecules, Nature 403 (2000) 635–638.
[6] M. Taniguchi, T. Kawai, DNA electronics, Physica E: Low-dimensional Systems and Nanostructures 33 (2006) 1–12.
[7] H.A. Wagenknecht, Electron transfer processes in DNA: mechanisms, biological relevance and applications in DNA analytics, Natural Product Reports 23 (2006) 973–1006.
[8] E. Yavin, A.K. Boal, J.K. Barton, Protein–DNA charge transport: redox activation of a DNA repair protein by guanine radical, Proceedings of the National Academy of Sciences of the United States of America 102 (2005) 3546–3551.
[9] I. Kratochvílová, T. Todorciuc, K. Král, H. Němec, M. Bunček, J. Šebera, S. Záliš, Z. Vokáčová, V. Sychrovský, L. Bednárová, P. Mojzeš, B. Schneider, Charge transport in DNA oligonucleotides with various base-pairing patterns, The Journal of Physical Chemistry. B 114 (2010) 5196–5205.
[10] D.B. Hall, R.E. Holmlin, J.K. Barton, Oxidative DNA damage through long-range electron transfer, Nature 382 (1996) 731–735.
[11] E.M. Conwell, S.M. Bloch, P.M. McLaughlin, D.M. Basko, Duplex polarons in DNA, Journal of the American Chemical Society 129 (2007) 9175–9181.
[12] F.D. Lewis, T. Wu, Y. Zhang, R.L. Letsinger, S.R. Greenfield, M.R. Wasielewski, Distance-dependent electron transfer in DNA hairpins, Science 277 (1997) 673–676.
[13] J.C. Genereux, S.M. Wuerth, J.K. Barton, Single-step charge transport through DNA over long distances, Journal of the American Chemical Society 133 (2011) 3863–3868.
[14] A. Heller, Spiers memorial lecture: on the hypothesis of cathodic protection of gene, Faraday Discussions 116 (2000) 1–13.
[15] E.C. Friedberg, DNA damage and repair, Nature 421 (2003) 436–440.
[16] S. Kanvah, G.B. Schuster, The sacrificial role of easily oxidizable sites in the protection of DNA from damage, Nucleic Acids Research 33 (2005) 5133–5138.
[17] I. Kratochvílová, K. Král, M. Bunček, A. Víšková, S. Nešpůrek, A. Kochalska, T. Todorciuc, M. Weiter, B. Schneider, Conductivity of natural and modified DNA measured by scanning tunneling microscopy. The effect of sequence, charge and stacking, Biophysical Chemistry 138 (2008) 3–10.
[18] L. Benda, M. Straka, V. Sychrovský, Y. Tanaka, On the role of mercury in the non-covalent stabilisation of consecutive U–Hg-II–U metal-mediated nucleic acid base pairs: metallophilic attraction enters the world of nucleic acids, Physical Chemistry Chemical Physics 13 (2011) 100–103.
[19] M.A. O'Neill, J.K. Barton, 2-aminopurine: a probe of structural dynamics and charge transfer in DNA and DNA: RNA hybrids, Journal of the American Chemical Society 124 (2002) 13053–13066.
[20] S.O. Kelley, J.K. Barton, Electron transfer between bases in double helical DNA, Science 283 (1999) 375–381.
[21] U. Wenge, J. Wengel, H.A. Wagenknecht, Photoinduced reductive electron transfer in LNA:DNA hybrids: a compromise between conformation and base stacking, Angewandte Chemie International Edition 51 (2012) 10026–10029.
[22] L.P. Candeias, S. Steenken, Structure and acid–base properties of one-electron-oxidized deoxyguanosine, guanosine, and 1-methylguanosine, Journal of the American Chemical Society 111 (1989) 1094–1099.
[23] J.T. Stivers, 2-Aminopurine fluorescence studies of base stacking interactions at abasic sites in DNA: metal-ion and base sequence effects, Nucleic Acids Research 26 (1998) 3837–3844.

[24] D.G. Xu, T.M. Nordlund, Sequence dependence of energy transfer in DNA oligonucleotides, Biophysical Journal 78 (2000) 1042–1058.
[25] T.M. Nordlund, D.G. Xu, K.O. Evans, Excitation energy transfer in DNA: duplex melting and transfer from normal bases to 2-aminopurine, Biochemistry 32 (1993) 12090–12095.
[26] R.A. Hochstrasser, T.E. Carver, L.C. Sowers, D.P. Millar, Melting of a DNA helix terminus within the active site of a DNA polymerase, Biochemistry 33 (1994) 11971–11979.
[27] O.F.A. Larsen, I.H.M. van Stokkum, B. Gobets, R. van Grondelle, H. van Amerongen, Probing the structure and dynamics of a DNA hairpin by ultrafast quenching and fluorescence depolarization, Biophysical Journal 81 (2001) 1115–1126.
[28] A. Noy, A. Perez, F. Lankaš, F.J. Luque, M. Orozco, Relative flexibility of DNA and RNA: a molecular dynamics study, Journal of Molecular Biology 343 (2004) 627–638.
[29] H.A. Wagenknecht, Charge Transfer in DNA: From Mechanism to Applications, WILLEY-WCH Verlag GmbH&Co KGaA, Wenheim, 2005.
[30] N. Valls, A. Santaolalla, J.L. Campos, J.A. Subirana, Packing features of the all-AT oligonucleotide d(AAATTT), Journal of Biomolecular Structure & Dynamics 24 (2007) 547–551.
[31] C. González, W. Stec, M.A. Reynolds, T.L. James, Structure and dynamics of a DNA·RNA hybrid duplex with a chiral phosphorothioate moiety: NMR and molecular dynamics with conventional and time-averaged restraints, Biochemistry 34 (1995) 4969–4982.
[32] E.J. Merino, A.K. Boal, J.K. Barton, Biological contexts for DNA charge transport chemistry, Current Opinion in Chemical Biology 12 (2008) 229–237.
[33] M. Vala, J. Vyňuchal, P. Toman, M. Weiter, S. Luňák Jr., Novel, soluble diphenyldiketo-pyrrolopyrroles: experimental and theoretical study, Dyes and Pigments 84 (2010) 176–182.
[34] S. Grimme, Semiempirical GGA-type density functional constructed with a long-range dispersion correction, Journal of Computational Chemistry 27 (2006) 1787–1799.
[35] S. Grimme, J. Antony, S. Ehrlich, H. Krieg, A consistent and accurate ab initio parametrization of density functional dispersion correction (DFT-D) for the 94 elements H–Pu, Journal of Chemical Physics 132 (2010) 154104.
[36] F. Weigend, R. Ahlrichs, Balanced basis sets of split valence, triple zeta valence and quadruple zeta valence quality for H to Rn: design and assessment of accuracy, Physical Chemistry Chemical Physics 7 (2005) 3297–3305.
[37] A. Schäfer, H. Horn, R. Ahlrichs, Fully optimized contracted Gaussian basis sets for atoms Li to Kr, Journal of Chemical Physics 97 (1992) 2571–2577.
[38] F. Furche, D. Rappoport, Density functional methods for excited states: equilibrium structure and electronic spectra, in: M. Olivucci (Ed.), Computational Photochemistry, vol. 16, Elsevier, Amsterdam, 2005, p. 93.
[39] F. Weigend, Accurate Coulomb-fitting basis sets for H to Rn, Physical Chemistry Chemical Physics 8 (2006) 1057–1065.
[40] A. Klamt, G. Schüürmann, COSMO: a new approach to dielectric screening in solvents with explicit expressions for the screening energy and its gradient, Journal of the Chemical Society, Perkin Transactions 2 (1993) 799–805.
[41] G. Scalmani, M.J. Frisch, Continuous surface charge polarizable continuum models of solvation. I. General formalism, Journal of Chemical Physics 132 (2010) 114110.
[42] R. Ahlrichs, M. Bar, M. Haser, H. Horn, C. Kolmel, Electronic structure calculations on workstation computers: the program system turbomole, Chemical Physics Letters 162 (1989) 165–169.
[43] Y. Zhao, N.E. Schultz, D.G. Truhlar, Design of density functionals by combining the method of constraint satisfaction with parametrization for thermochemistry, thermochemical kinetics, and noncovalent interactions, Journal of Chemical Theory and Computation 2 (2006) 364–382.
[44] Y. Zhao, D.G. Truhlar, Density functionals with broad applicability in chemistry, Accounts of Chemical Research 41 (2008) 157–167.
[45] P.C. Hariharan, J.A. Pople, The influence of polarization functions on molecular orbital hydrogenation energies, Theoretica Chimica Acta 28 (1973) 213–222.
[46] M.J. Frisch, et al., Gaussian 09, Revision A02, Gaussian Inc., Wallinford, CT, 2009.
[47] A.D. Becke, A new mixing of Hartree–Fock and local density — functional theories, Journal of Chemical Physics 98 (1993) 1372–1377.
[48] C.T. Lee, W.T. Yang, R.G. Parr, Development of the Colle–Salvetti correlation-energy formula into a functional of the electron density, Physical Review B 37 (1998) 785–789.
[49] J. Nožár, S. Nešpůrek, J. Šebera, Polaron binding energy in polymers: poly [methyl(phenyl)silylene], Journal of Molecular Modeling 8 (2012) 623–629.
[50] E.M. Conwell, Charge transport in DNA in solution: the role of polarons, Proceedings of the National Academy of Sciences of the United States 102 (2005) 8795–8799.
[51] E.M. Conwell, J. Park, H. Choi, Polarons in DNA: transition from guanine to adenine transport, The Journal of Physical Chemistry. B 109 (2005) 9760–9763.
[52] T. Kubař, M. Elstner, Coarse-grained time-dependent density functional simulation of charge transfer in complex systems: application to hole transfer in DNA, The Journal of Physical Chemistry. B 114 (2010) 11221–11240.
[53] D.M. Basko, E.M. Conwell, Effect of solvation on hole motion in DNA, Physical Review Letters 88 (2002) 098102-1–098102-4.
[54] R.J. Cave, M.D. Newton, Generalization of the Mulliken–Hush treatment for the calculation of electron transfer matrix elements, Chemical Physics Letters 249 (1996) 15–19.
[55] R.J. Cave, M.D. Newton, Calculation of electronic coupling matrix elements for ground and excited state electron transfer reactions: comparison of the generalized Mulliken–Hush and block diagonalization methods, Journal of Chemical Physics 106 (1997) 9213–9226.
[56] A.A. Voityuk, Electronic couplings in DNA pi-stacks: multistate effects, The Journal of Physical Chemistry. B 109 (2005) 17917–17921.
[57] A.K. Siriwong, A.A. Voityuk, Electron transfer in DNA, Wiley Interdisciplinary Reviews — Computational Molecular Science 2 (2012) 780–794.
[58] D. Beljonne, G. Pourtois, M.A. Ratner, J.L. Bredas, Pathways for photoinduced charge separation in DNA hairpins, Journal of the American Chemical Society 125 (2003) 14510–14517.
[59] J.R. Zheng, Y.K. Kang, M.J. Therien, D.N. Beratan, Generalized Mulliken–Hush analysis of electronic coupling interactions in compressed pi-stacked porphyrin-bridge-quinone systems, Journal of the American Chemical Society 127 (2005) 11303–11310.
[60] M.D. Newton, Quantum chemical probes of electron-transfer kinetics: the nature of donor–acceptor interactions, Chemical Reviews 91 (1991) 767–792.
[61] L. Blancafort, A.A. Voityuk, CASSCF/CAS-PT2 study of hole transfer in stacked DNA nucleobases, Journal of Physical Chemistry A 110 (2006) 6426–6432.
[62] D. Řeha, W. Barford, S. Harris, A multi-scale method for the calculation of charge transfer rates through the Pi-stack of DNA: application to DNA dynamics, Physical Chemistry Chemical Physics 10 (2008) 5436–5444.
[63] T. Uchiyama, T. Miura, H. Takeuchi, T. Dairaku, T. Komuro, T. Kawamura, Y. Kondo, L. Benda, V. Sychrovský, P. Bouř, I. Okamoto, A. Ono, Y. Tanaka, Raman spectroscopic detection of the T–Hg–II–T base pair and the ionic characteristics of mercury, Nucleic Acids Research 40 (2012) 5766–5774.
[64] Z. Vokáčová, M. Buděšinský, I. Rosenberg, B. Schneider, J. Šponer, V. Sychrovský, Structure and dynamics of the ApA, ApC, CpA, and CpC RNA dinucleoside monophosphates resolved with NMR scalar spin–spin couplings, The Journal of Physical Chemistry. B 113 (2009) 1182–1191.
[65] M. Tanaka, B. Elias, J.K. Barton, DNA-mediated electron transfer in naphthalene-modified oligonucleotides, Journal of Organic Chemistry 75 (2010) 2423–2428.
[66] I. Rosenberg, in: R.F. Schinazi, Liotta (Eds.), Frontiers in Nucleosides and Nucleic Acids, IHL Press, 2004, pp. 519–548.
[67] R. Liboska, J. Snášel, I. Barvík, M. Buděšínský, R. Pohl, Z. Točík, O. Páv, D. Rejman, P. Novák, I. Rosenberg, 4′-Alkoxy oligodeoxynucleotides: a novel class of RNA mimics, Organic & Biomolecular Chemistry 9 (2011) 8261–8267.
[68] H. Němec, I. Kratochvílová, J. Šebera, A. Kochalska, J. Nožár, S. Nešpůrek, Charge carrier mobility in poly[methyl(phenyl)silylene] studied by time-resolved terahertz spectroscopy and molecular modelling, Physical Chemistry Chemical Physics 13 (2011) 2850–2856.
[69] V. Petráková, A.J. Taylor, I. Kratochvílová, F. Fendrych, J. Vacík, J. Kučka, J. Štursa, P. Cígler, M. Ledvina, A. Fišerová, P. Kneppo, M. Nesládek, Luminescence of nanodiamond driven by atomic functionalization: towards novel biomolecular detection principles, Advanced Functional Materials 22 (2012) 812–819.